

Research Article

Accuracy and precision of ^{31}P -MRS assessment for evaluating the effect of melatonin-pretreated mitochondria transferring on liver fibrosis of rats

Sheung-Fat Ko¹, Tien-Hung Huang^{2,3,4}, Yuan-Ping Lin⁵, Yi-Ling Chen^{2,3,4}, Hon-Kan Yip^{*2,3,4,6,7,8}

¹Department of Radiology; ²Division of Cardiology, Department of Internal Medicine, Kaohsiung Chang Gung Memorial Hospital and Chang Gung University College of Medicine, Kaohsiung, 83301, Taiwan

³Institute for Translational Research in Biomedicine; ⁴Center for Shockwave Medicine and Tissue Engineering, Kaohsiung Chang Gung Memorial Hospital, Kaohsiung 83301, Taiwan

⁵3R Life Sciences Ltd, Kaohsiung, 82144, Taiwan.

⁶Department of Medical Research, China Medical University Hospital, China Medical University, Taichung 40402, Taiwan

⁷Department of Nursing, Asia University, Taichung 41354, Taiwan;

⁸Division of Cardiology, Department of Internal Medicine, Xiamen Chang Gung Hospital, Xiamen 361028, Fujian, China

*Correspondence: rylchen.msu@gmail.com, Tel: 886-77317123 ext.8961; han.gung@msa.hinet.net, Tel: 886-77317123 ext.8300.

Running title: Quantitative ^{31}P -MRS for detecting hepatic fibrosis

Received: January 2, 2022; Accepted: March 9, 2022

ABSTRACT

This study examined the reliability of ^{31}P phosphorus-magnetic resonance spectroscopy (^{31}P -MRS) to measure parameters of liver metabolic function in the intact animals. These parameters can help us to evaluate the severity and prognosis of liver fibrosis. In addition, ^{31}P -MRS was also used to examine the protective effects of melatonin on liver mitochondria. An animal model of liver fibrosis was established via intraperitoneal administration of thioacetamide (TAA) to rats. Rats were scanned at baseline, week 3 and 6 after TAA treatment, respectively, to measure the longitudinal changes of phosphorus metabolite levels by ^{31}P -MRS at 9.4 T. The results showed a consistent decline in the levels of phosphorus metabolites (inorganic phosphate, α -ATP, γ -ATP and NADH) in rats with fibrosis. Impaired mitochondrial respiration capacity, collagen accumulation and the extent of fibrosis in liver were markedly associated with decreased concentrations of phosphorus metabolites. Melatonin-pretreated mitochondria transferring efficiently prevented TAA-induced liver damage mainly by restoring mitochondrial function. In conclusion, the levels of phosphorus metabolites could serve as the indicators of mitochondrial oxidative capacity and thus provides a novel tool to evaluate mitochondrial integrity in the *in vivo* condition by using ^{31}P -MRS in the setting of liver fibrosis.

Key words: magnetic resonance image, fibrosis, ATP synthesis, mitochondrial function

1. INTRODUCTION

The initiation of hepatic fibrosis is an important pathological alteration for the most chronic liver diseases (1-3). Liver biopsy is considered the gold standard for the diagnosis of cirrhosis and the classification of fibrosis by direct visual evaluation of total amount and distribution of fibrous tissue (4-6). However, biopsy is invasive with a relatively high risk of complications (7). Although conventional radiological examinations, including ultrasonography and computed tomography, offers the potential for noninvasive diagnosis, staging, and monitoring of liver fibrosis (8-10), these techniques are primarily dependent on the detection of morphological changes in the liver, and these changes are usually detected in advanced (end-stage) liver fibrosis or cirrhosis (11). When the fibrosis progresses to advanced liver disease, liver transplantation appears as the last lifesaving resource, but it is suffered by limited organ resources and high cost (12). Therefore, the development of quantitative, reliable, and sensitive diagnostic tools including assessing hepatic energy metabolism and mitochondrial functional integrity to monitor the progression of liver disorders is essential.

Magnetic resonance imaging (MRI) and magnetic resonance spectroscopy (MRS) provide the unique opportunity for a noninvasive *in vivo* assessment of tissue metabolism without suffering ionizing radiation. In addition to the information of static spectra, phosphorous-31 MRS (³¹P-MRS) also offers an unique method for the assessment of the levels of chemical reactions which are involved in energy metabolism (13). Of particular interest is that this modality can also accurately investigate the mitochondrial oxidative phosphorylation in the *in vivo* conditions, from the metabolite concentrations to metabolic fluxes via adenosine-triphosphate (ATP)-generating enzymes (14-16). Liver is rich in mitochondria which have distinct characteristics compared to other organs' mitochondria, since they are the axis that link the hepatic metabolism of carbohydrates, lipids, and proteins. Mitochondria are also critical in hepatocyte survival as a mediator of apoptosis and necrosis (17). Therefore, there is adequate reason to doubt a mitochondrial dysfunction in liver parenchyma (18, 19).

Melatonin is the major product of the pineal gland and it also acts as an antioxidant by scavenging reactive oxygen species (ROS) (20). Melatonin also maintains the optimal mitochondrial membrane potential and preserves mitochondrial integrity (21, 22). However, it remains unclear whether melatonin-pretreated mitochondria exert the hepatic-protective effects on liver fibrosis. Therefore, in this study, thioacetamide (TAA) will be used to establish a rat model of liver fibrosis which will be monitored by ³¹P-MRS. The apparent diffusion coefficient (ADC) quantified from diffusion weighted imaging (DWI) MR imaging will serve as *in vivo* quantitative technique to accurately predict the process of fibrosis. In addition, whether the melatonin-pretreated mitochondria transferring into the TAA-treated rats preserves the mitochondrial integrity against liver cirrhosis will be examined.

2. MATERIALS AND METHODS

2.1. Ethics statement.

Animal studies were conducted and approved by Institute of Animal Care and Use Committee at Kaohsiung Chang Gung Memorial Hospital (Affidavit of Approval of Animal Use Protocol No. 2017112902). All experiments were carried out following Guide for the Care and Use of Laboratory Animals, 8th edition.

2.2 Animal model of liver fibrosis.

Adult male Sprague–Dawley (SD) rats (8 weeks and 250 ± 20 g), were purchased from the BioLASCO Taiwan Co., Ltd (Taiwan). Rats were housed at $25 \pm 3^\circ\text{C}$ with 12/12 hours light/dark and allowed to access to food and tap water freely. The animals were divided into four groups, i.e., (1) control rats (received vehicle only), (2) TAA for 3-week rats, (3) TAA for 6-week rats and (4) TAA + melatonin-pretreated mitochondrial-transferred rats. In the present study, the TAA rats received intraperitoneal injection of TAA (200 mg/kg of body weight) 3 times weekly for 6 consecutive weeks. Additionally, the TAA + melatonin-pretreated mitochondria rats received TAA injection for 3 weeks, followed by intravenous injection of melatonin-pretreated mitochondria (1 mg) weekly for another 3 consecutive weeks. The dosage of mitochondria utilized in the present study was based on previous studies with some modifications (21-23). At the end of 6 weeks after liver fibrosis induction, rats were euthanized to analyze their serum biochemistry, liver histopathology, mitochondrial function for the purposes of confirming the severity and the effect of melatonin-pretreated mitochondria transferring on liver fibrosis.

2.3. Isolation of melatonin-pretreated mitochondria.

In brief, rats received an intraperitoneal injection of melatonin (50 mg/kg) at 6 and 18 hours prior to euthanasia and starved overnight. After euthanasia, the liver was harvested and immediately immersed in ice-cold IB buffer for homogenization. The mitochondria were isolated from homogenates by differential centrifugation described earlier (20-23). The 10 mg of isolated mitochondria were labeled with $1 \mu\text{M}$ of MitoTracker Red CMXRos (Thermo Fisher Scientific, Carlsbad, CA) through incubation at 37°C for 30 min. These mitochondria were referred as “melatonin-pretreated mitochondria”. After MitoTracker labeling, these mitochondria were quickly transfused into the recipient animals (i.e., less than 3 hours for preparation).

2.4. Magnetic resonance imaging assessment.

The liver MRI were analyzed by a 9.4T horizontal-bore animal MR scanning system (Biospec 94/20, Bruker, Ettingen, Germany) which comprises a self-shielded magnet with a 20 cm clear bore and a BGA-12S gradient insert (inner diameter: 12 cm) that offered a maximal gradient strength of 675 mT/m. After anesthesia with inhalation of 2% isoflurane, the rats were kept in shallow breathing and placed in the prone position. T2-weighted associated with DWI MR imaging was performed with transmitter-receiver volume coil for signal detection from rat liver. For ^{31}P -MRS, a $^1\text{H}/^{31}\text{P}$ dual-tuned surface coil (20 mm in diameter) tuned to 400.3 and 161.9 MHz was used to study the proton imaging and phosphorus spectroscopy for covering whole liver area on rat. The protocols of MRI pulse sequences, including T2-weighted imaging for hepatic anatomic details, DWI and ADC measurements for Brownian motion of water molecules, and ^{31}P -MRS for energy metabolism have been described in our previous study (23).

2.5. Histopathological analysis.

Tissue sections were fixed, embedded, sectioned, stained with hematoxylin and eosin (H&E) or mason’s trichrome staining to detect hepatic injury and collagen fibers, and the images were taken by an optical microscope (Olympus) described previously (22, 23). The degree of liver

injury was assessed based on published standards (22, 23). Masson's trichrome staining were used for determining liver fibrosis. The integrated area (μm^2) of the fibrotic area on each section was calculated using the Image Tool 3 (IT3) image analysis software (UTHSA). After H&E staining, the degree of liver injury was assessed with liver injury score defined as follows: 0 – No notable hepatocyte integrity impairment or sinusoidal distortion; 1 – Mild hepatic injury with less than 25% of the section involved; 2 – Moderate hepatic injury with 25–50% of the section involved; 3 – Severe hepatic injury with more than 50% involved.

Immunohistochemical staining for expressions of α -smooth muscle actin (SMA) (1:400; Abcam) and tissue inhibitors of metalloproteinase (TIMP)-2 (1:100; Abcam) were performed with primary antibody anti- α -SMA (Sigma) and secondary antibody anti-mouse polyvalent-PE conjugate (Sigma-Aldrich) incubating for 30 minutes at room temperature. Irrelevant antibody will be used as a control. For each rat, three liver sections were examined, and three randomly selected high-power fields (HPFs) (i.e., 100x) were analyzed in each section. The mean number per HPF for each animal was then determined by the summation of all numbers divided by 9.

2.6. Western blot analysis.

Total protein extracts were loaded and polyvinylidene fluoride (PVDF) membranes were blocked overnight in Tris-buffered saline-Tween 20 buffer, 5% non-fat milk, followed by hybridization with primary antibodies Total OXPHOS Rodent WB Antibody Cocktail (Abcam) in the same buffer. The proteins were detected with enhanced chemiluminescence (ECL) reagents (Amersham Biosciences). Densitometric evaluation was performed with Image J.

2.7. Seahorse XF Cell Mito stress test.

The Seahorse XF24 Extracellular Flux Analyzer (Agilent) was used to measure the O_2 consumption rate (OCR), an indicator of mitochondrial respiration, and the extracellular acidification rate (ECAR), an indicator of glycolysis, in isolated mitochondria. Quantifications of OCR and ECAR were based on our previous reports (22, 24, 25). The O_2 consumption, ATP-linked respiration, proton leak respiration, maximal respiration, and spare respiratory capacity, were derived by the sequential addition of four compounds (Oligomycin, FCCP, antimycin A, rotenone) to the respiring cells, respectively following the manufacturer's instructions.

2.8. Statistical analysis.

Quantitative data were expressed as means \pm SD. Statistical analysis was performed by AVOVA followed by unpaired student t-test using SAS statistical software for Windows version 8.2 (SAS institute, Cary, NC). A probability value <0.05 was considered statistically significant.

3. RESULTS

3.1. Effects of thioacetamide (TAA) treatment on liver fibrosis in rats.

At the end of the study (6 weeks), the liver tissues were examined. In TAA treated rats, the liver gross appearance showed the formation of small nodules on the outer surface of liver. There was no significant disparity between TAA 3- and 6-week rats in parenchyma sizes and rough

surfaces (figure 1A-D). As shown in figure 1E-G, the levels of AST, ALT, and ALP were normal in TAA rats. Additionally, the serum levels of pro-inflammatory cytokines, transforming growth factor (TGF)- β 1 and interleukin (IL)-6, were in the TAA rats was significantly increased compared to the control rats (figure 1H-I), IL-6 did not significantly differ among the 3 groups

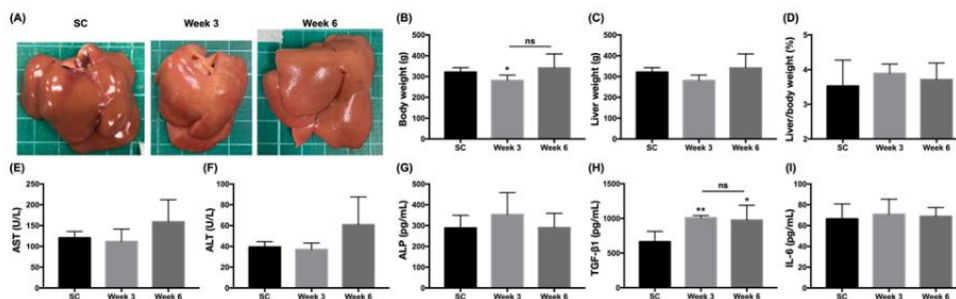


Fig. 1. Effects of TAA on gross appearance and physiological functions of rat liver.

(A) Images of gross appearance, control (sc) showing regular smooth surface, TAA 3-week and TAA 6-week rat showing liver with nodular surface and a nearly smooth surface. (B-D) Body weight, liver weight and relative weights of liver. (E-I) levels of serum aspartate transferase (AST), alanine transferase (ALT), alkaline phosphatase (ALP), transforming growth factor (TGF)- β 1 and interleukin (IL)-6. $n=6$. * $P<0.05$; **, $P<0.01$ vs control.

3.2. Magnetic resonance image (diffusion-weighted image) assessment of liver fibrosis.

Comparing axial T2-weighted with DWI MR imaging showed an irregular liver outline in TAA treated rats, which also returned higher signal intensity compared with normal liver parenchyma due to impeded water diffusion (figure 2A-B). ADC is a quantitative parameter of water molecules within tissue and is commonly computed using DWI MR imaging. As shown in figure.2C, the ADC values were decreased as liver fibrosis progressed in TAA rats.

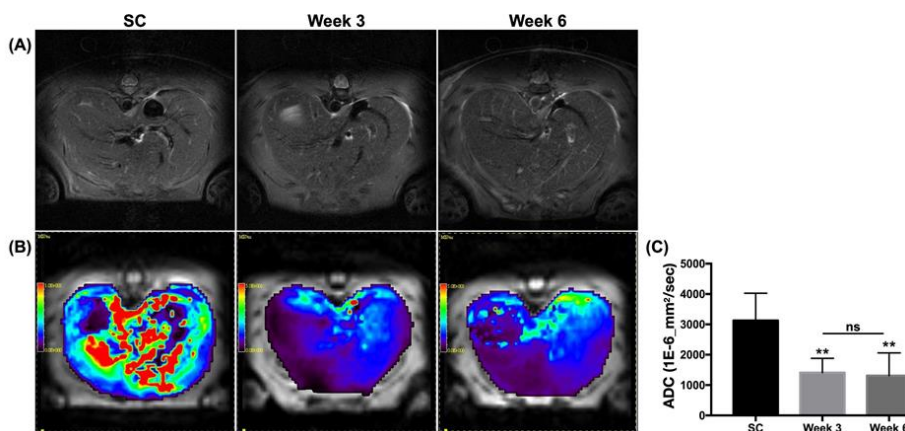


Fig. 2. Assessment of DWI MR imaging and ADC in rat liver fibrosis induced by TAA.

(A) T2-weighted and (B) DWI MR imaging of the liver in control (SC) and TAA rats. In TAA rats, the Brownian motion of water molecules is restricted in highly cellular tissue (blue: restricted diffusion). Control rats have fewer barriers to water mobility and the apparent diffusion is relatively free (red/yellow/green: facilitated diffusion). (C) Mean values of ADC in left and right lobes. $n=6$. ** $P<0.01$ vs control, ns, non-significant difference.

3.3. Histological examination of liver fibrosis induced by TAA in rats.

Under H&E and Masson's trichrome staining, the fibrosis with hepatocyte necrosis and mild leucocyte infiltration of liver parenchyma in TAA was observed compared to the control rats (figure 3A-B). In the TAA rats, the collagen fibers were accumulated with the formation of fibrous septa surrounding the hepatic lobules compared with the control rats (figure 3C-D). The fibrosis-relevant gene expressions were also examined. As shown in figure 3E-F, the expressions of α -smooth muscle actin (α -SMA), and tissue inhibitor of metalloproteinases-2 (TIMP-2) were significantly increased in the liver parenchyma of TAA rats compared with control rats (figure 3G-H). Correlation analysis (Table 1) revealed no significant associations between ADC and hepatic α -SMA expression ($r=-0.39$, $p=0.14$). Significant correlations existed between the ADC and hepatic TIMP-2 expression ($r=-0.53$, $p=0.04$) and collagen deposition ($r=-0.51$, $p<0.04$).

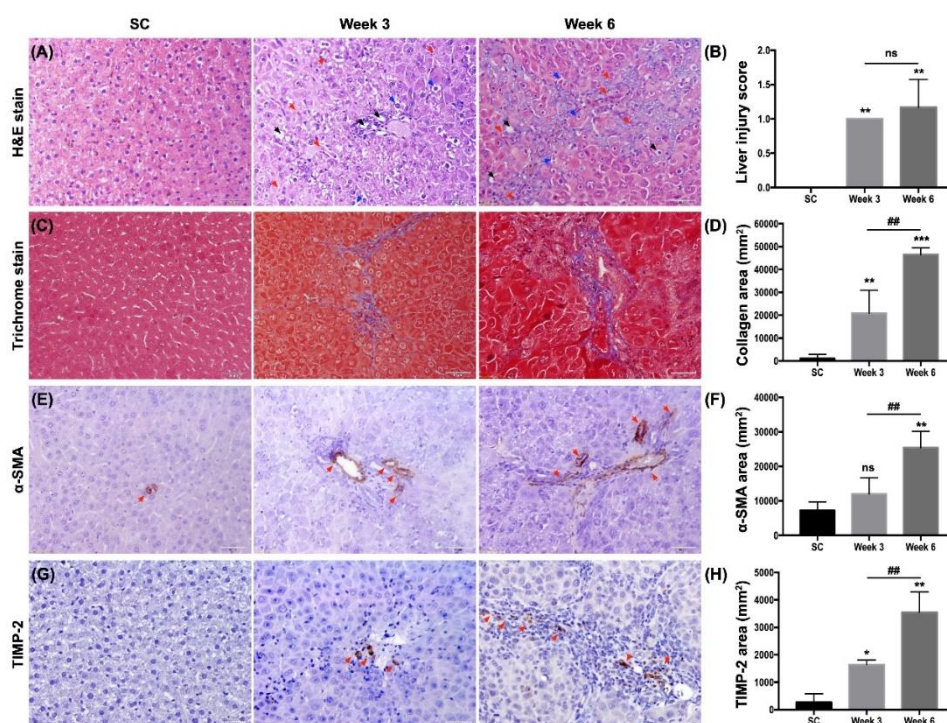


Fig. 3. Histological assessments of rat liver fibrosis induced by TAA.

(A) H&E staining of hepatic tissue in TAA 3- and 6-week rats showed hepatocytes degeneration (blue arrow), infiltration of inflammatory cells (red arrow), and vacuolated cells (black arrow) $\times 100$. (B) Liver injury scores. (C) Masson's trichrome staining for; increased fibrosis, and blue collagen fibers were seen among hepatocytes and portal area (central vein) in TAA rats, $\times 100$. (D) Quantification of fibrotic area as expressed by the percentage of blue pixels per field. (E) Immunohistochemical staining for α SMA. α -SMA positive cell were significantly increased in TAA rats (red arrow), $\times 100$. (F) Quantification of α -SMA positive cells as expressed by the percentage of brown pixels per field. (G) Immunohistochemical staining for TIMP-2. TIMP-2 positive cells were significantly increased in TAA rats (red arrow), $\times 100$. (H) Quantification of TIMP-2 positive cells as expressed by the percentage of brown pixels per field. $n=6$. * $P<0.05$; **, $P<0.01$; ***, $P<0.001$ vs control; ns, non-significant difference. ## $P<0.01$ as TAA 3-week vs TAA 6-week rats. ns, non-significant difference. SC, sham control.

Table 1. Correlations between hepatic phosphorous metabolites, apparent diffusion coefficient, and immunohistochemistry staining in thioacetamide induced liver fibrosis.

	Correlation (r)	p Value
α-SMA		
Pi	-0.38	0.15
NADH	-0.51	0.04*
γ -ATP	-0.19	0.47
α -ATP	-0.33	0.21
ADC	-0.39	0.14
TIMP-2		
Pi	-0.43	0.11
NADH	-0.62	0.01*
γ -ATP	-0.39	0.15
α -ATP	-0.37	0.17
ADC	-0.53	0.04*
Masson's trichrome stain		
Pi	-0.51	0.04*
NADH	-0.62	0.01*
γ -ATP	-0.40	0.13
α -ATP	-0.47	0.06
ADC	-0.51	0.04*

ADC, apparent diffusion coefficient; α -SMA, α -smooth muscle actin; TIMP-2, tissue inhibitor of metalloproteinases-2; Pi, inorganic phosphate; ATP, adenosine-triphosphate; NADH, NADH dehydrogenase.

3.4. ^{31}P -magnetic resonance spectroscopy assessment of hepatic phosphorus metabolites in rats.

^{31}P -MRS was used to assess mitochondrial metabolism of liver in vivo. At 3 and 6 weeks after TAA treatment, a substantial change in the signal of phosphorus metabolites was observed in the ^{31}P -MRS (figure.4A). The levels of various phosphorus metabolites related to β -ATP were presented in Table 2. The level of phosphomonoester (PME) showed a slight upward trend with liver fibrosis progression (figure.4B). On the other hand, the levels of inorganic phosphate (Pi), α -ATP, γ -ATP, and NADH dehydrogenase (complex I) were significantly decreased in rats treated with TAA. The levels of phosphorus metabolites were significantly lower in the TAA 3-week rats as compared to the other two groups (fig.4C-F), however, there were no significant differences in NADH and α -ATP between TAA 3-week rats and TAA 6-weeks rats (figure 4D-E).

Correlation analysis (Table 2) showed no significant associations between these hepatic phosphorous metabolite levels (i.e., γ -ATP, α -ATP, and Pi) and hepatic expressions of α -SMA and TIMP-2, but Pi levels did correlate with collagen deposition area ($r=-0.51$, $p<0.004$). Hepatic NADH level also correlated with hepatic expressions of α -SMA ($r=-0.51$, $p<0.004$), TIMP-2 ($r=-0.62$, $p<0.01$) as well as collagen deposition area ($r=-0.62$, $p<0.01$).

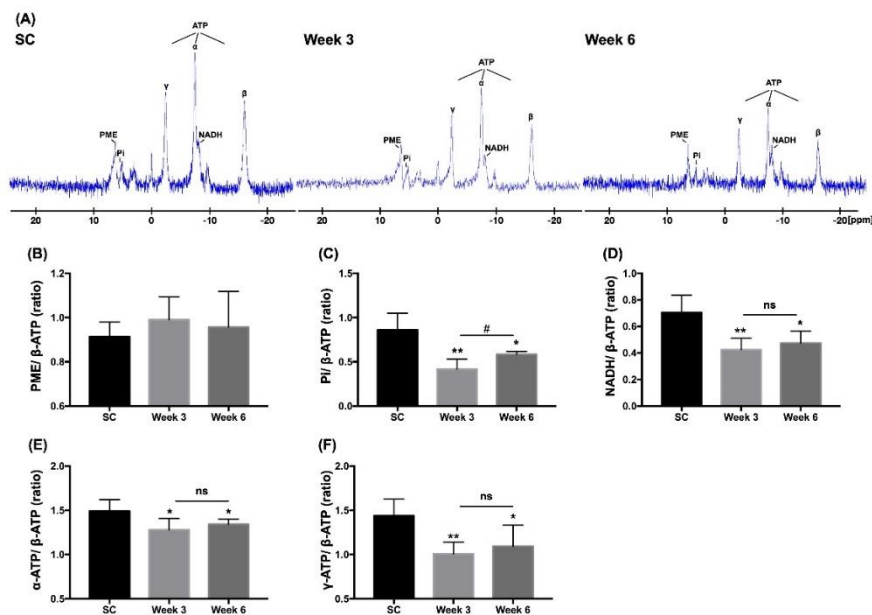


Fig. 4. Assessment of impaired mitochondrial energy metabolism in liver of TAA rats at ³¹P-magnetic resonance spectrum-9.4T.

(A) Representative hepatic ³¹P-magnetic resonance spectrum at 9.4T of livers of control and TAA treated rats. (B-G) The relative levels of phosphorus metabolites were subtracted from the β-ATP value. The quantitative data represent the mean ± SD (n=6). * P<0.05; ** P<0.01 vs control; ns, non-significant difference. #P<0.05 as TAA 3-week vs TAA 6-week rat. ns. ATP, adenosine triphosphate; NADH, nicotinamide adenine dinucleotide. Pi, inorganic phosphate; PME, phosphomonoesters. SC, sham control.

Table 2. Relative levels of hepatic phosphorylated metabolites in control rats and rats at various stages of TAA induced liver fibrosis.

Week	PME	Pi	γ-ATP	α-ATP	NADH
0	0.91±0.07	0.86±0.19	1.44±0.13	1.49±0.13	0.70±0.13
3	0.99±0.10	0.42±0.11***	1.01±0.13***	1.28±0.13*	0.42±0.09***
6	0.96±0.16	0.58±0.03	1.23±0.04	1.34±0.06	0.47±0.09**

PME, phosphomonoester; Pi, inorganic phosphate; ATP, adenosine-triphosphate; NADH, NADH dehydrogenase. β-ATP as internal control. Mean ± SD. Significant differences from the SC group at *, P<0.05; **, P<0.01; ***, P<0.001.

3.5. Examination (Seahorse XF Cell Mito stress test) of mitochondrial function in rats.

By directly measuring the oxygen consumption rate (OCR) of cells, the Seahorse XF Cell Mito Stress Test was used to assess the effect of TAA on the mitochondrial respiration. The mitochondrial respiration after sequential injection of oligomycin (a complex V inhibitor), carbonyl cyanide-4-(trifluoromethoxy) phenylhydrazone (FCCP; a protonophore) and a combination of antimycin A and rotenone (inhibitors of complex III and I) were depicted in figure

5. The mitochondrial respiration of hepatocytes was compromised starting at TAA 3-weeks. These were reflected in a decreased ATP-linked respiration, proton leak respiration, spare respiratory capacity, and especially in maximal respiration during TAA administration. Maximal respiratory capacity was estimated by an FCCP-stimulated respiration and its decrease is a strong indicator of potential mitochondrial dysfunction (figure 5A-E).

To assess whether TAA influenced the mitochondrial oxidative phosphorylation (i.e., OXPHOS) system in hepatic mitochondria of TAA rats, the expressions of various subunits of the electron transport chain (ETC; mitochondrial complexes I–IV) was measured by western blot analysis. The decreased expressions of mitochondrial ETC complexes were observed in TAA 3-week and TAA 6-week rats compared to control rats, (figure 5F-K). These results indicated that TAA directly inhibited mitochondrial function starting from 3 weeks, including impairment in ATP-linked respiration, proton leak, maximal respiration, and spare respiratory capacity.

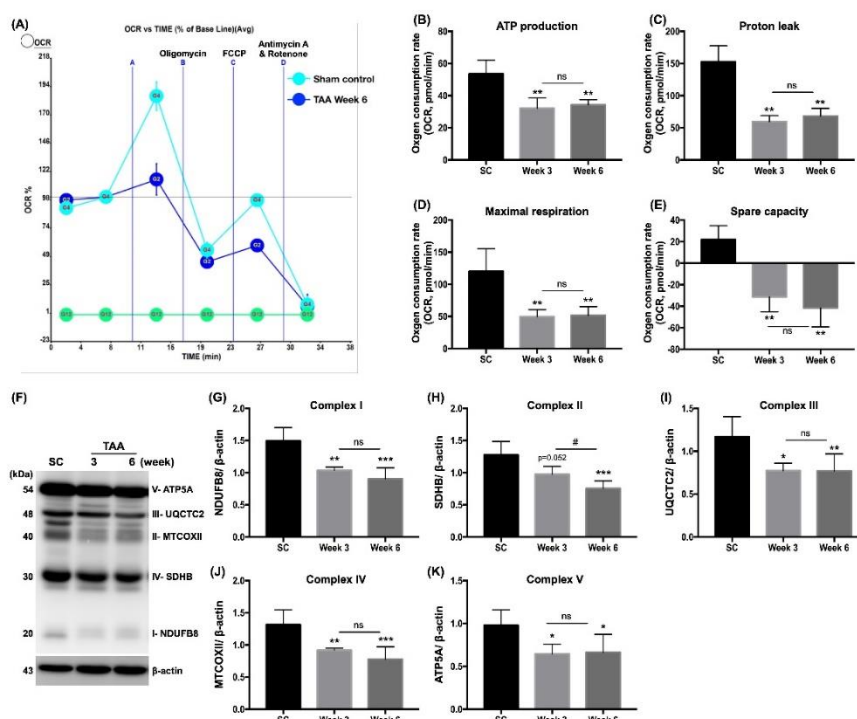


Fig. 5. Mitochondrial dysfunction in liver of thioacetamide administered rats.

Seahorse XF Cell Mito Stress Test was performed to measure control rats and TAA rats following a sequential addition of inhibitors of mitochondrial function: oligomycin, FCCP, and a combination of rotenone and antimycin A. (A) OCR profile plot, (B) ATP-linked respiration, (C) Proton leak respiration, (D) Maximal respiration, and (E) Spare respiratory capacity. ATP-linked respiration and proton leak respiration were calculated following the addition of oligomycin. Maximal respiration was measured following the addition of FCCP. Spare respiratory capacity was calculated based on the difference between the basal respiration and maximal respiration. (F) Representative western blot for mitochondrial oxidative phosphorylation complexes in liver of control, TAA 3-week, and TAA 6-week rats. (G-K) Quantitative determination of mitochondrial complex subunits was normalized to β -actin. $n=6$. * $P<0.05$; ** $P<0.01$; *** $P<0.001$ vs control; ns, non-significant difference. ## $P<0.01$ as TAA 3-week vs TAA 6-week rats, SC, sham control; TAA, thioacetamide.

Correlations between hepatic phosphorous metabolites, and seahorse parameters in TAA treated rats were presented in Table 3. Hepatic NADH level correlated with seahorse parameters [i.e., ATP production ($r=0.54$, $p=0.04$), proton leak ($r=0.76$, $p=0.01$), maximal respiration ($r=0.61$, $p=0.02$), and spare respiratory capacity ($r=0.63$, $p=0.01$)]. Hepatic Pi level correlated with both maximal respiration ($r=0.63$, $p=0.01$) and spare capacity ($r=0.60$, $p=0.02$).

Table 3. Correlations between hepatic phosphorous metabolites, and seahorse parameters in thioacetamide induced liver fibrosis.

	Correlation (r)	p Value
ATP production		
Pi	0.62	0.01*
NADH	0.54	0.04*
γ -ATP	0.69	0.01*
α -ATP	0.58	0.03*
Proton leak		
Pi	0.68	0.01*
NADH	0.76	0.01*
γ -ATP	0.67	0.01*
α -ATP	0.58	0.03*
Maximal respiration		
Pi	0.63	0.01*
NADH	0.61	0.02*
γ -ATP	0.59	0.03*
α -ATP	0.49	0.07
Spare respiratory capacity		
Pi	0.60	0.02*
NADH	0.63	0.01*
γ -ATP	0.53	0.05
α -ATP	0.46	0.09

Pi, inorganic phosphate; ATP, adenosine-triphosphate; NADH, NADH dehydrogenase.

3.6. Effects of melatonin-pretreated mitochondria transferring on the mitochondrial function in the liver of TAA treated rats.

To further investigate whether melatonin-pretreated mitochondria transferring alleviate mitochondrial dysfunction and maintain mitochondrial quality in TAA treated rats, we measured the liver mitochondrial function following by the melatonin-pretreated mitochondria transferring into the TAA treated rats. The results showed an improvement in the phosphorus metabolite profiles in the liver, measured by ^{31}P -MRS-9.4T after mitochondrial transferring (figure 6). TAA week-6 rats have the significantly lower values of Pi, α -ATP, γ -ATP, and NADH dehydrogenase (P-trend: 0.0003 for Pi; P-trend: 0.0046 for γ -ATP; P-trend: 0.0002 for α -ATP and NADH) than the control rats. However, the rats with melatonin-pretreated mitochondria transferring had significantly increased values of Pi, α -ATP, γ -ATP, and NADH dehydrogenase and these values were comparable to levels of control rats (figure.6C-F). As expected, melatonin-pretreated mitochondria transferring restored the ability of mitochondrial respiration, including ATP-linked

respiration, proton leak respiration, spare respiratory capacity, and maximal respiration (figure.6G-K), as well as rescued the decrease in ETC complex protein subunit expression (mitochondrial complexes I–IV) in rats treated with TAA (figure.6L-Q).

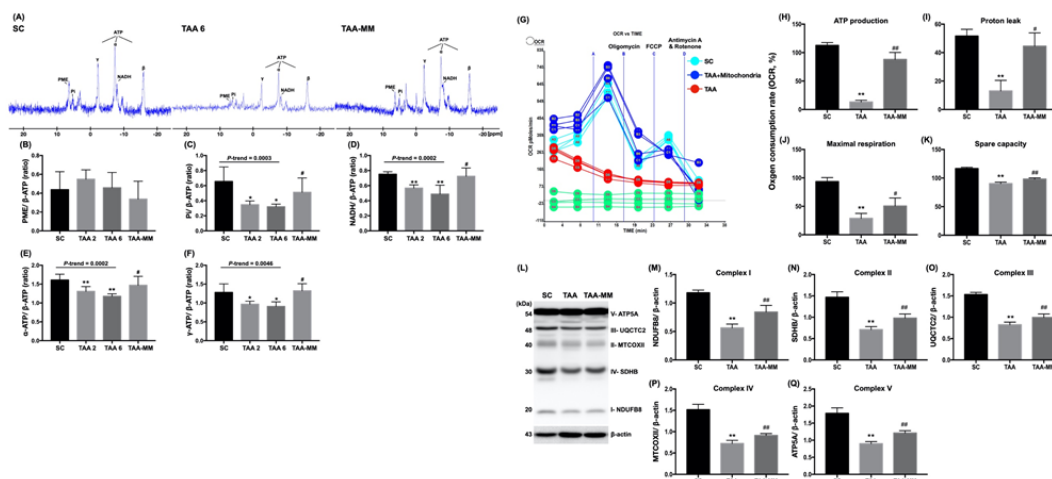


Fig. 6. Effects of melatonin-pretreated mitochondria transferring on mitochondrial energy metabolism and respiration measured by ^{31}P -MRS-9.4T

(A) Hepatic ^{31}P -MRS-9.4T graphs of mitochondrial metabolisms. (B-F) The phosphorus metabolite levels normalized to β -ATP. $n=5$. (G) OCR profile, (H) ATP-linked respiration, (I) Proton leak respiration, (J) Maximal respiration, and (K) Spare respiratory capacity. Seahorse analyzer assay showed restoring mitochondria function in TAA treated rats with melatonin-pretreated mitochondria transferring. (L) Images of western blot for mitochondrial oxidative phosphorylation complexes in livers. (M-Q) Quantitative analyses of mitochondrial complex subunits normalized to β -actin. $n=6$. * $P<0.05$; ** $P<0.01$ vs control, # $P<0.05$; ## $P<0.01$ vs TAA alone rat. SC, sham control; TAA, thioacetamide; MM, melatonin-pretreated mitochondria.

4. DISCUSSION

This study reported that ^{31}P -MRS-9.4T could be used to monitor the longitudinal changes from the molecular to anatomical microstructural levels of the liver fibrosis in rats. The results indicated that this method could provide several important preclinical information. By use of this method, the significant changes in hepatic energy metabolism and mitochondrial respiration capacity as well as mitochondrial oxidative phosphorylation have been uncovered in the liver cirrhosis progression. Interestingly, the alterations in hepatic phosphorus metabolites (i.e., Pi, α/γ -ATPs, and NADH) were correlated with the alterations in liver function and histopathology. Therefore; hepatic ^{31}P -MRS-9.4T provided a non-invasive means to detect the severity and progression of liver fibrosis. The data also showed that in the early phase of liver fibrosis, the physiological and biochemical parameters exhibited no significant difference between the control rats and the rats treated with TAA which eventually would cause liver fibrosis. Of important finding was that the melatonin-pretreated mitochondria transferring into the TAA treated rats could improve mitochondrial function indicated by the increased intracellular ATP content and metabolic activity. Thus, this transferring efficiently prevented TAA-induced liver fibrosis by improving endogenous mitochondrial functional integrity. Collectively, ^{31}P -MRS-9.4T can be used for basic research and clinical diagnosis on the liver function at the *in vivo* condition.

TAA is widely used to study the liver fibrosis, because of its accurate simulation of the underlying mechanisms involved in human liver fibrosis (26). Prolonged TAA treatment caused extreme fibrosis and cirrhosis around 12-16 weeks in rats and 16-24 weeks in mice (27-30). The initiation of fibrogenesis by TAA is a slow process, but followed by a sudden acceleration of extracellular matrix deposition to a steady state level (29, 30). It is well known that liver fibrosis is an essential development for hepatocellular carcinoma (HCC). The degree of fibrosis is positively correlated to HCC (1). As a result, early detection of HCC is critical for the effective or even curable treatment and also can prolong survival time for patients.

ALT and AST serum levels are most used in both clinical diagnosis and basic research involving liver injury (31, 32). Because TAA causes hepatocyte injury (33), plasma membrane damage and protein leakage of hepatocytes, thus, it elevates activities of hepato-specific enzymes including AST, ALT, and ALP. However, in the current study, we found that TAA did not significantly elevate ALT and AST. These findings suggested that these conventional parameters may not be sufficient to serve as the precise biomarkers for evaluating the early phase of liver damage. On other hand, H&E staining, mason's trichrome staining, α -SMA and TIMP-2 for fibrosis degree and the accumulation of collagen fiber exhibited a positive correlation to the disease progression. Currently, biopsy and pathohistological findings have been regarded as the "gold standard" in the diagnosis of liver fibrosis, as confirmed in this study. However, biopsy is invasive with potential complications including pain, procedure-related bleeding, infection and even mortality (5, 34). In addition, the variability in limited tissue samplings and difficulty in long-term follow-up are the limitation of this modality in the daily clinical practice (5, 34).

Other image tools, such as MRI, computed tomography, and ultrasound, have been frequently used in the diagnosis of HCC, but their limitations are often to miss detecting and characterizing small lesion (≤ 2 cm) in the cirrhotic liver (35-37). In the present study, we showed the advantage of ^{31}P -MRS-9.4T with its sensitivity and reliability for detecting the liver fibrosis and liver cirrhosis. Additionally, the ^{31}P -MRS-9.4T is able to detect alterations of phosphorus metabolites in liver tissue, including α/γ -ATP, Pi, and NADH. Moreover, our results also demonstrated that ^{31}P -MRS-9.4T provided a powerful tool in vivo assessment of hepatic metabolism as early as in the initial stage of fibrotic lesions. The unique noninvasive nature of ^{31}P -MRS-9.4T allows the longitudinal tracking of fibrotic progression by repeated measurements. It also can be used to underly mechanisms of fibrogenesis, to identify possible therapeutic targets and intervention time point, as well as to directly assess the effect of antifibrotic therapies.

In previous study, we found that a quantitative ^{31}P -MRS measurement in liver parenchyma offered a promising tool to detect hepatic metabolic alternations in rats with hepatic ischemia reperfusion injury (23). Here, we also demonstrated that the quantitative ^{31}P -MRS spectrum in combination with Seahorse analyzer assay (i.e., measurement of oxygen consumption rate) and expression of oxidative phosphorylation components (i.e., mitochondrial complex I-V) were able to detect mitochondrial abnormalities in liver parenchyma at early phase of liver fibrogenesis. Our findings highlighted that ^{31}P -MRS was a reliable and sensitive tool for assessing mitochondrial function and hepatic energy metabolism at 9.4-Tesla MRI facility.

Melatonin is the major product of the pineal gland and it also acts as an antioxidant by scavenging reactive oxygen species (38-41). Melatonin maintains the optimal mitochondrial membrane potential and preserves mitochondrial functions (42, 43). Interestingly, melatonin pretreatment enhanced the function of isolated mitochondria against several chemical insults [Supplemental figure 1]. An intriguing finding was that when the melatonin-pretreated mitochondria was transferred into the animals who were suffered mitochondrial damage caused

by TAA in liver, the damaged mitochondria were rescued by this transferring. The results suggested that melatonin-pretreated mitochondria benefit to the liver against hepatic ischemia-reperfusion injury (14, 21, 22, 44) and also in TAA-induced liver fibrosis in the present study.

We realized that despite extensive works were done in the present *in vitro* and *in vivo* studies, the precise mechanisms for how the melatonin-pretreated mitochondrial therapy to improve the hepatocyte mitochondrial function in the TAA-induced fibrosis chain model remains to be clarified. Although our previous study (45) demonstrated that melatonin treatment enhanced mitochondrial transfer from normal neurons to mitochondria-depleted neurons (i.e., by cell-to-cell transfer) mainly through the tunneling nanotubes, this study did not repeat previous one (45) to prove whether the exogenous mitochondrial transfer could incorporate into the damaged cells caused by TAA, including those of hepatocytes and stellate cells.

In conclusion, we demonstrated that ^{31}P -MRS-9.4T can provide robust phosphorus metabolic information (i.e., the levels of PME, Pi, α/γ -ATPs, and NADH) at an early stage of liver fibrosis. Therefore, we encourage that ^{31}P -MRS-9.4T should be started to use in the early assessment of liver fibrogenesis in the daily clinical practice. By use of ^{31}P -MRS-9.4T, we also found that melatonin-pretreated mitochondria transferring could offer a synergic benefit on protecting the liver against TAA-induced liver fibrosis (figure 7).

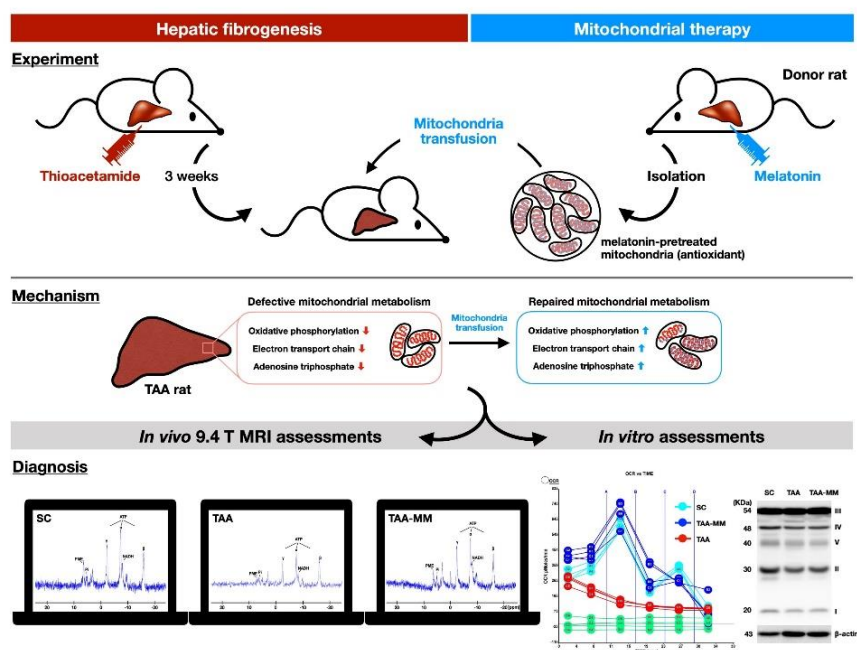


Fig. 7. The potential mechanisms of melatonin-pretreated mitochondria transferring on the progression of hepatic fibrogenesis induced by TAA.

A novel approach of mitotherapy (isolated melatonin-pretreated mitochondria) recovered the mitochondrial oxidative phosphorylation, and improved the ATP synthesis in mitochondria, and consequently restore hepatocyte function in TAA treated rats. ^{31}P -MRS provided reproducible and experimentally useful measures of phosphorus metabolites and mitochondrial function in hepatic fibrosis. ATP, adenosine triphosphate; MM, melatonin-pretreated mitochondria; MRI, magnetic resonance imaging; NADH, nicotinamide adenine dinucleotide; Pi, inorganic phosphate; PME, phosphomonoesters; SC, sham control; TAA, thioacetamide; I-V; complex I-V of the electron transport chain.

LIST OF ABBREVIATIONS

apparent diffusion coefficient (ADC); adenosine-triphosphate (ATP); diffusion weighted imaging (DWI); extracellular acidification rate (ECAR); electron transport chain (ETC); hematoxylin and eosin (H&E); oxygen consumption rate (OCR); oxidative phosphorylation (OXPHOS); ³¹P-magnetic resonance spectroscopy (³¹P-MRS); inorganic phosphate (Pi); phosphomonoester (PME); α -smooth muscle actin (SMA); thioacetamide (TAA); transforming growth factor- β 1 (TGF- β 1); tissue inhibitors of metalloproteinase 2 (TIMP-2)

ACKNOWLEDGEMENTS

This research was funded by the following grants and agencies: Ministry of Science and Technology Taiwan (MOST 107-2314-B-182A-061 MY2) and Chang Gung Memorial Hospital, Chang Gung University (NMRPG8H6021, NMRPG8H6022). We thank the molecular imaging core of the Institute for Translational Research in Biomedical Sciences, Kaohsiung Chang Gung Memorial Hospital, Kaohsiung, Taiwan for technical and facility supports on 9.4T animal MRI.

AUTHORSHIP

Conceptualization, SFK and YLC; Methodology, Investigation, Formal Analysis, and Data Curation, THH, YPL and YLC; Writing – Original Draft Preparation, YLC; Writing – Review & Editing, SFK and HKY; Project Administration and Funding Acquisition, SFK.

CONFLICT INTERESTS

The authors declare that there is no conflict of interest regarding the publication of this paper.

REFERENCES

1. Li C, Li R, Zhang W (2018) Progress in non-invasive detection of liver fibrosis. *Cancer Biol. Med.* **15** (2): 124-136.
2. Bataller R, Brenner DA (2005) Liver fibrosis. *J. Clin. Invest.* **115** (2): 209-218.
3. Abdel-Misih SR, Bloomston M (2010) Liver anatomy. *Surg. Clin. North Am.* **90** (4): 643-653.
4. Schmeltzer PA, Talwalkar JA (2011) Noninvasive tools to assess hepatic fibrosis: ready for prime time? *Gastroenterol. Clin. North Am.* **40** (3): 507-521.
5. Bedossa P, Paradis V (2003) Liver extracellular matrix in health and disease. *J. Pathol.* **200** (4): 504-515.
6. Bedossa P, Carrat F (2009) Liver biopsy: the best, not the gold standard. *J. Hepatol.* **50** (1): 1-3.
7. Janes CH, Lindor KD (1993) Outcome of patients hospitalized for complications after outpatient liver biopsy. *Ann. Intern Med.* **118** (2): 96-98.
8. Cardi M, et al. (1997) Superiority of laparoscopy compared to ultrasonography in diagnosis of widespread liver diseases. *Dig. Dis. Sci.* **42** (3): 546-548.
9. Li S, et al. (2019) Liver fibrosis conventional and molecular imaging diagnosis update. *J. Liver.* **8** (1): 236.

10. Kudo M, *et al.* (2008) Diagnostic accuracy of imaging for liver cirrhosis compared to histologically proven liver cirrhosis. A multicenter collaborative study. *Intervirolgy* **51** (Suppl 1): 17-26.
11. Yeom SK, Lee CH, Cha SH, Park CM (2015) Prediction of liver cirrhosis, using diagnostic imaging tools. *World J. Hepatol.* **7** (17): 2069-2079.
12. Samuel D, Feray C, Bismuth H (1997) Hepatitis viruses and liver transplantation. *J. Gastroenterol. Hepatol.* **12** (9-10): S335-341.
13. Prompers JJ, *et al.* (2006) Dynamic MRS and MRI of skeletal muscle function and biomechanics. *NMR Biomed.* **19** (7): 927-953.
14. Valkovic L, Chmelik M, Krssak M (2017) In-vivo ³¹P-MRS of skeletal muscle and liver: A way for non-invasive assessment of their metabolism. *Anal. Biochem.* **529**: 193-215.
15. Liu Y, Gu Y, Yu X (2017) Assessing tissue metabolism by phosphorous-31 magnetic resonance spectroscopy and imaging: a methodology review. *Quant. Imaging Med. Surg.* **7** (6): 707-726.
16. Corbin IR, *et al.* (2003) Hepatic ³¹P MRS in rat models of chronic liver disease: assessing the extent and progression of disease. *Gut* **52** (7): 1046-1053.
17. Degli Esposti D *et al.* (2012) Mitochondrial roles and cytoprotection in chronic liver injury. *Biochem. Res. Int.* 2012: 387626.
18. Lane M, *et al.* (2016) Mitochondrial dysfunction in liver failure requiring transplantation. *J. Inherit. Metab. Dis.* **39** (3): 427-436.
19. Rahman S (2013) Gastrointestinal and hepatic manifestations of mitochondrial disorders. *J. Inherit. Metab. Dis.* **36** (4): 659-673.
20. Reiter RJ, *et al.* (2003) Melatonin as an antioxidant: biochemical mechanisms and pathophysiological implications in humans. *Acta Biochim. Pol.* **50** (4): 1129-1146.
21. Sun CK, *et al.* (2015) Systemic combined melatonin-mitochondria treatment improves acute respiratory distress syndrome in the rat. *J. Pineal Res.* **58** (2): 137-150.
22. Chen HH, *et al.* (2016) Melatonin pretreatment enhances the therapeutic effects of exogenous mitochondria against hepatic ischemia-reperfusion injury in rats through suppression of mitochondrial permeability transition. *J. Pineal Res.* **61** (1): 52-68.
23. Ko SF, *et al.* (2020) Hepatic ³¹P-magnetic resonance spectroscopy identified the impact of melatonin-pretreated mitochondria in acute liver ischaemia-reperfusion injury. *J. Cell Mol. Med.* **24** (17):10088-10099.
24. Sun CK, *et al.* (2017) Melatonin treatment enhances therapeutic effects of exosomes against acute liver ischemia-reperfusion injury. *Am. J. Transl. Res.* **9** (4): 1543-1560.
25. Tahan V, *et al.* (2004) Melatonin reduces dimethylnitrosamine-induced liver fibrosis in rats. *J. Pineal Res.* **37** (2): 78-84.
26. Yang HY *et al.* (2019) Dendropanax morbifera ameliorates thioacetamide-induced hepatic fibrosis via TGF-beta1/Smads pathways. *Int. J. Biol. Sci.* **15** (4): 800-811.
27. Reif S, *et al.* (2004) Treatment of thioacetamide-induced liver cirrhosis by the Ras antagonist, farnesylthiosalicylic acid. *J. Hepatol.* **41** (2): 235-241.
28. Wallace MC, *et al.* (2015) Standard operating procedures in experimental liver research: thioacetamide model in mice and rats. *Lab. Anim.* **49** (1 Suppl): 21-29.
29. Delire B, Starkel P, Leclercq I (2015) Animal models for fibrotic liver diseases: What we have, what we need, and what is under development. *J. Clin. Transl. Hepatol.* **3** (1): 53-66.

30. Salguero Palacios R et al. (2008) Activation of hepatic stellate cells is associated with cytokine expression in thioacetamide-induced hepatic fibrosis in mice. *Lab. Invest.* **88** (11): 1192-1203.
31. Amin A, Mahmoud-Ghoneim D (2011) Texture analysis of liver fibrosis microscopic images: a study on the effect of biomarkers. *Acta Biochim. Biophys. Sin.* **43** (3): 193-203.
32. Sathesh Kumar S, Ravi Kumar B, Krishna Mohan G (2009) Hepatoprotective effect of *Trichosanthes cucumerina* Var *cucumerina* L. on carbon tetrachloride induced liver damage in rats. *J. Ethnopharmacol.* **123** (2): 347-350.
33. Chen TM, Subeq YM, Lee RP, Chiou TW, Hsu BG (2008) Single dose intravenous thioacetamide administration as a model of acute liver damage in rats. *Int. J. Exp. Pathol.* **89** (4): 223-231.
34. Jeantet AY, Truchet M, Naulleau G, Martoja R (1991) Effects of bromadiolone on some organs and tissues (liver, kidney, spleen, blood) of coypu (*Myocastor coypus*). *C. R. Acad. Sci. III.* **312** (4): 149-156.
35. Bargellini I, et al. (2014) Radiological diagnosis of hepatocellular carcinoma. *J. Hepatocell Carcinoma* **1**: 137-148.
36. Schraml C, et al. (2015) Imaging of HCC-current state of the art. *Diagnostics* (Basel). **5** (4): 513-545.
37. Ariff B, et al. (2009) Imaging of liver cancer. *World J. Gastroenterol.* **15** (11): 1289-1300.
38. Reiter RJ, et al. (2016) Melatonin as an antioxidant: under promises but over delivers. *J. Pineal Res.* **61** (3): 253-278.
39. Reiter RJ, et al. (2017) Melatonin as a mitochondria-targeted antioxidant: one of evolution's best ideas. *Cell Mol. Life Sci.* **74** (21): 3863-3881.
40. Tan DX, Reiter RJ (2020) An evolutionary view of melatonin synthesis and metabolism related to its biological functions in plants. *J. Exp. Bot.* **71** (16): 4677-4689.
41. Fu Z, et al. (2020) Cardioprotective Role of melatonin in acute myocardial infarction. *Front. Physiol.* **11**: 366.
42. Tan DX, Manchester LC, Qin L, Reiter RJ (2016) Melatonin: A Mitochondrial Targeting Molecule Involving Mitochondrial Protection and Dynamics. *Int. J. Mol. Sci.* **17** (12): 2124.
43. Zhao D, et al. (2019) Melatonin synthesis and function: Evolutionary history in animals and plants. *Front. Endocrinol.* (Lausanne). **10**: 249.
44. Ma Z, et al. (2017) Melatonin and mitochondrial function during ischemia/reperfusion injury. *Cell Mol. Life Sci.* **74** (21): 3989-3998.



This work is licensed under a [Creative Commons Attribution 4.0 International License](https://creativecommons.org/licenses/by/4.0/)

Please cite this paper as:

Ko, S.-F., Huang, T.-H., Lin, Y.-P., Chen, Y.-L. and Yip, H.-K., 2022. Accuracy and precision of ^{31}P -MRS assessment for evaluating the effect of melatonin-pretreated mitochondria transferring on liver fibrosis of rats. *Melatonin Research*. **5**, 1 (Mar. 2022), 18-33. DOI:<https://doi.org/https://doi.org/10.32794/mr112500117>.